

**Use of a biojective direct search
algorithm in the process design of
material science applications**

A.E. Gheribi, J.-Ph. Harvey, E. Bélisle,
C. Robelin, P. Chartrand, A.D. Pelton,
C.W. Bale, S. Le Digabel

G-2014-103

December 2014

Revised: August 2015

Les textes publiés dans la série des rapports de recherche *Les Cahiers du GERAD* n'engagent que la responsabilité de leurs auteurs.

La publication de ces rapports de recherche est rendue possible grâce au soutien de HEC Montréal, Polytechnique Montréal, Université McGill, Université du Québec à Montréal, ainsi que du Fonds de recherche du Québec – Nature et technologies.

Dépôt légal – Bibliothèque et Archives nationales du Québec, 2015.

The authors are exclusively responsible for the content of their research papers published in the series *Les Cahiers du GERAD*.

The publication of these research reports is made possible thanks to the support of HEC Montréal, Polytechnique Montréal, McGill University, Université du Québec à Montréal, as well as the Fonds de recherche du Québec – Nature et technologies.

Legal deposit – Bibliothèque et Archives nationales du Québec, 2015.

Use of a biobjective direct search algorithm in the process design of material science applications

Aïmen E. Gheribi^a

Jean-Philippe Harvey^b

Ève Bélisle^c

Christian Robelin^a

Patrice Chartrand^a

Arthur D. Pelton^a

Christopher W. Bale^a

Sébastien Le Digabel^d

^a CRCT, Centre de recherche en calcul thermochimique, Département de génie chimique, Polytechnique Montréal, Montréal (Québec) Canada, H3C 3A7

^b Department of Mining and Materials Engineering, McGill University, Montréal (Québec) Canada, H3A 2B2

^c School of Information Technology and Electrical Engineering, The University of Queensland, Brisbane, QLD 4072, Australia

^d GERAD & Département de mathématiques et de génie industriel, Polytechnique Montréal, Montréal (Québec) Canada, H3C 3A7

aimen.gheribi@polymtl.ca, jean-philippe.harvey@mail.mcgill.ca
e.belisle@uq.edu.au, christian.robelin@polymtl.ca
patrice.chartrand@polymtl.ca, arthur.pelton@polymtl.ca
cbale@polymtl.ca, sebastien.le.digabel@gerad.ca

December 2014

Revised: August 2015

Les Cahiers du GERAD

G–2014–103

Copyright © 2015 GERAD

Abstract: This work describes the application of a direct search method to the optimization of problems of real industrial interest, namely three new material science applications designed with the **FactSage** software. The search method is BiMADS, the biobjective version of the mesh adaptive direct search (MADS) algorithm, designed for blackbox optimization. We give a general description of the algorithm, and, for each of the three test cases, we describe the optimization problem, discuss the algorithmic choices, and give numerical results to demonstrate the efficiency of BiMADS for real cases of alloy and process design.

Key Words: Blackbox optimization, derivative-free optimization, biobjective optimization, mesh adaptive direct search, material science, alloy design, process design.

Acknowledgments: The work of the first, fifth, and sixth authors was supported by a grant from the Natural Sciences and Engineering Research Council of Canada (NSERC) via the Magnesium Strategic Research Network. The last author was supported by NSERC grant 418250 and by AFOSR FA9550-12-1-0198.

The authors thank Christopher Hutchinson and Chad Sinclair for their approach to the steel-design problem, which allowed us to test BiMADS on this complex application.

1 Introduction

We consider the following biobjective problem:

$$\min_{x \in \Omega} F(x) = (f^{(1)}(x), f^{(2)}(x)) \quad (1)$$

where $\Omega = \{x \in \mathcal{X} : c_j(x) \leq 0, j \in J\} \subset \mathbb{R}^n$ defines the feasible region; $f^{(1)}, f^{(2)}, c_j : \mathcal{X} \rightarrow \mathbb{R} \cup \{\infty\}$ for all $j \in J = \{1, 2, \dots, m\}$; and \mathcal{X} is a subset of \mathbb{R}^n .

Problem (1) is a *blackbox optimization problem* because the objectives and constraint functions are seen as *blackboxes* or as functions of the outputs of a blackbox. No analytical expression is available for a blackbox; it is typically the result of a computer simulation. It may have several characteristics that are problematic for optimization, including noise and uncertainty, nonsmoothness, the presence of many local optima, and hidden constraints that cause the simulation to fail for otherwise feasible designs. It can also be expensive to execute. In this context, we must find a feasible solution in Ω with minimal values for the objectives, given a limited *budget of evaluations*. Gradient-based methods are inappropriate because first-order information is unavailable, and approximating this information is not practical since the approximation may be inaccurate and/or too expensive to obtain with regard to the number of evaluations.

Hence, *derivative-free optimization* [14] may be considered, and in particular the biobjective variant of the *mesh adaptive direct search* (MADS) [4] algorithm, called the BiMADS algorithm [7]. These methods are specialized for blackbox optimization and are available through the NOMAD solver [1, 26]. This choice was motivated by considering a number of requirements for the solver. It had to be freely available, easily coupled with the FactSage software [9], and applicable to biobjective problems. It also had to provide default values for all the algorithmic parameters and handle constraints via a built-in strategy,

Several freely distributed solvers satisfy some of these requirements, including the genetic algorithms NSGA-II [16] and AMGA2 [35] and the direct multisearch (DMS) method [15]. If in addition we consider that, ideally, the algorithm underlying the solver should possess a mathematical proof of convergence, then only NOMAD satisfies all the requirements. We will however compare NOMAD to the NSGA-II heuristic in one of the examples.

In the present study, we are interested in the application of BiMADS to three new problems in material science with two conflicting objectives. They all use the FactSage software, which consists of a series of calculation and manipulation modules accessing various pure-substance and solution databases. Users have access to databases of thermodynamic data for thousands of compounds, as well as optimized databases for hundreds of metallic, oxide, and salt solutions (solid and liquid). The databases were developed by the modeling and optimization of phase equilibria and thermodynamic data. The FactSage software accesses these databases to calculate phase diagrams and the conditions for phase equilibria in multicomponent systems. The software has many useful features. It can for example follow the course of equilibrium or Scheil–Gulliver cooling, predict the freezing range, segregate the alloying elements and phase formation with the accompanying volume and enthalpy changes, and calculate the amounts of the various precipitates during the subsequent annealing. For instance, one can search for alloys within a given composition range, with various options such as a liquidus temperature below a certain limit, a desired freezing range, a maximum or minimum amount of precipitate after annealing at a given temperature, or a density or shrinkage ratio within a given range. One can also search for optimal annealing or rolling temperatures. However, for a multicomponent alloy, launching thousands of calculations over a grid of compositions is time-consuming or even impossible depending on the number of components. In previous work [21–23] we have demonstrated the ability of the MADS and BiMADS algorithms to solve simple alloy design problems with two objectives subject to several nonlinear constraints. In this work, we develop a similar approach for alloy/process design in real industrial applications.

The paper is organized as follows. Section 2 describes the BiMADS algorithm for biobjective optimization. Sections 3, 4, and 5 each discuss an application. The example in Section 3 demonstrates the applicability of BiMADS to optimizations involving phase equilibria, and the other two examples are realistic biobjective applications. Finally, Section 6 presents a discussion.

2 The BiMADS algorithm for biobjective optimization

We focus on BiMADS, which uses the MADS algorithm to solve the biobjective problem (1). MADS is designed for single-objective optimization and is briefly presented in Section 2.1. The NOMAD [1,26] software package implements both algorithms and is freely available under the LGPL license at www.gerad.ca/nomad. All the algorithmic features presented in this section are available in NOMAD and have been applied to the three applications described in Sections 3, 4, and 5. We used NOMAD version 3. NOMAD is coded in standard C++ and does not depend on any external library, so it was straightforward to link it to the FactSage software using the NOMAD *library mode* and an interface based on Windows DLLs.

2.1 The MADS algorithm

The MADS algorithm [4] is designed for single-objective optimization. It is a *direct search* method generalizing the *coordinate search* (CS) [19] and the *generalized pattern search* (GPS) [36] algorithms. At each iteration of the algorithm, *trial points*, or *candidates*, are generated on a spatial discretization called the *mesh*, and the functions defining the blackbox are evaluated at these locations. Depending on the success of these evaluations, the coarseness of the discretization is updated.

Each iteration is decomposed into two main steps: the *poll* and the *search*. The poll generates mesh trial points using directions from the current best solution. When normalized, the set of all MADS directions forms a dense set in the unit sphere.

While the poll step is rigidly defined in order to ensure convergence, the search step is more flexible. It generates mesh trial points using any appropriate method, provided these candidates are finite in number and on the current mesh. We used four types of searches for this work. First, *speculative search* [26] is the simplest and probably the most efficient strategy. It occurs after a successful poll in the previous iteration, and it generates a trial point further along the same successful direction. Other strategies include *latin hypercube sampling* (LHS) search, *variable neighborhood search* (VNS) [3], and quadratic-model search [13]. The speculative and quadratic-model searches are enabled by default in NOMAD and are used in all the tests of this paper. The LHS and VNS searches are used when specified.

Finally, constraints are handled by the *progressive barrier* (PB) approach [5]. PB is not a penalty method but is instead based on a constraint-violation function that defines a filter inspired by [20]. For further details of the MADS algorithm see [2–6, 13, 26].

2.2 The BiMADS algorithm

The BiMADS algorithm is described in [7]; it focuses on the biobjective optimization problem (1). Typically, the two objectives $f^{(1)}$ and $f^{(2)}$ are contradictory: a decrease in one causes an increase in the other, and it is unlikely that a unique point in Ω optimizes both objectives. A solution is then represented as a set of points in Ω called the *trade-off solution* or the *Pareto set*.

We use the following definition of dominance: $x \in \Omega$ dominates $y \in \Omega$, denoted $x \prec y$, if and only if $F(x) \leq F(y)$ and $f^{(q)}(x) < f^{(q)}(y)$ for at least one index q in $\{1, 2\}$. A solution $x \in \Omega$ is said to be *Pareto optimal* if there is no point $y \in \Omega$ such that $y \prec x$. The Pareto set is the set of Pareto solutions in Ω , and its image under F in the objective space in \mathbb{R}^2 is called the *Pareto front*.

The BiMADS method is a general framework that provides a set of nondominated solutions approximating the Pareto set. It does so by iteratively applying MADS to a series of single-objective reformulations of (1). The purpose of each of these reformulations is to improve a specific part of the approximated Pareto front. This has the following form:

$$\phi_r(F(x)) = \begin{cases} -\prod_{q=1}^2 (r_q - f^{(q)}(x))^2 & \text{if } F(x) \leq r, \\ \sum_{q=1}^2 ((f^{(q)}(x) - r_q)_+)^2 & \text{otherwise,} \end{cases}$$

where $r = (r_1, r_2) \in \mathbb{R}^2$ is the *reference point* defined in the objective space. This reformulation is such that $\phi_r(x) = 0$ if $x_1 = r_1$ or $x_2 = r_2$, with $x = (x_1, x_2)$; $\phi_r(x) > 0$ if $r \prec x$; and $\phi_r(x) < 0$ if $x \prec r$.

As a consequence, the optimization of ϕ_r on Ω , with r as a starting solution, potentially generates a solution that dominates r . This optimization is performed by MADS with the PB to treat the constraints of Ω . This concept is illustrated in Figure 1.

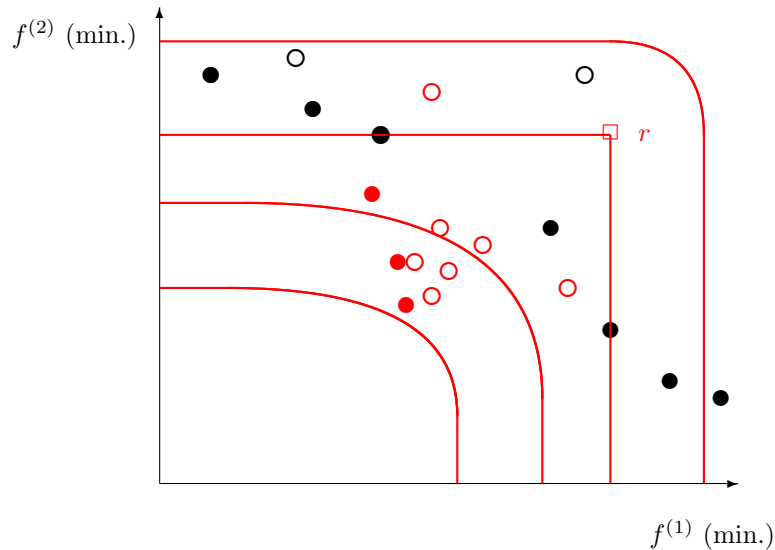


Figure 1: Illustration of the single-objective reformulation in the objective space. The curves represent the ϕ_r contours. At the reference point r , $\phi_r(r) = 0$, and for any point $x \in \Omega$ that dominates r , $\phi_r(x) < 0$. Red circles represent the evaluations performed by the single-objective optimization of ϕ_r . Filled red circles correspond to the new nondominated points, and filled black circles are the previous nondominated points.

The advantage of this reformulation based on a reference point is that any part of the Pareto front can be reached with some appropriate reference point; this is not the case when weights are placed on the objectives.

For efficiency, the reference point must be chosen such that the minimization of the associated reformulation will generate as many nondominated solutions as possible. BiMADS identifies the largest “hole” in the front, by first ordering the set of current nondominated solutions by $f^{(1)}$ value, and then for each triplet of successive points (x, y, z) finding the one that maximizes the distance $\|y - x\|^2 + \|z - y\|^2$. When this triplet $(\tilde{x}, \tilde{y}, \tilde{z})$ has been identified, the reference point is taken as $r = (\tilde{z}_1, \tilde{x}_2)$, with $\tilde{x} = (\tilde{x}_1, \tilde{x}_2)$ and $\tilde{z} = (\tilde{z}_1, \tilde{z}_2)$. In addition, a weight is associated with the reference point so that it is unlikely that the same point will be chosen again in the case of disconnected Pareto fronts.

In contrast to the other elements of the algorithm, the selection of the reference point is specific to the biobjective case, and thus BiMADS cannot be applied to problems with more than two objectives. A more general approach is the MultiMADS algorithm [8].

The general BiMADS framework is given in Figure 2. It begins with the individual minimizations of $f^{(1)}$ and $f^{(2)}$ so that a first rough approximation is available to help us choose the first reference point for the third single-objective optimization.

The convergence theory for MADS and BiMADS is explained in [4, 5, 7]. The analyses are presented as a hierarchy of results depending on the degree of smoothness of the problem. Most of these results are based on the Clarke calculus for nonsmooth functions [12]. Under some assumptions, in the single-objective case, global convergence to points satisfying local optimality conditions is achieved. With two objectives, it can be proved that moving in a feasible direction deteriorates at least one objective.

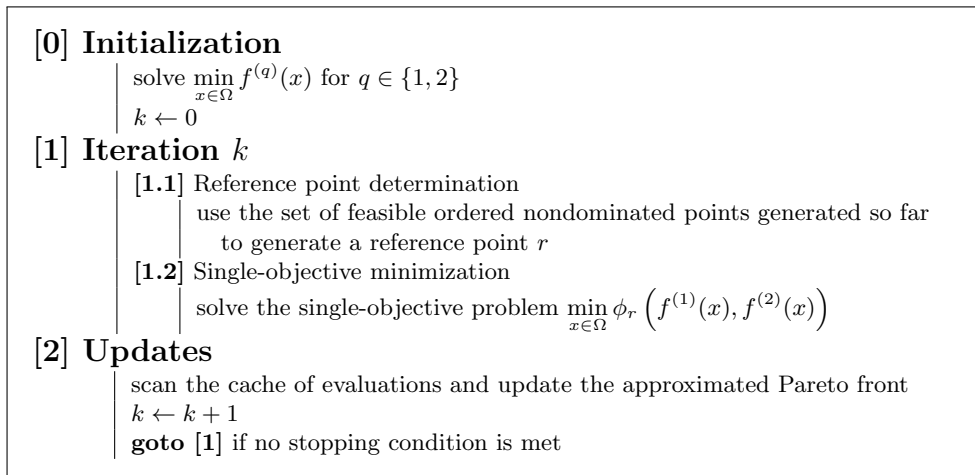


Figure 2: General description of the BiMADS algorithm.

3 Overall composition for minimum liquidus temperature and maximum heat capacity per volume

Recently, interest in molten salts has heightened. This is primarily due to research into sustainable solutions for renewable and green energies because of both environmental concerns and the decrease of the fossil-fuel reserve. Molten salts can be used in technology for latent heat energy storage, which is one of the most important components of a solar-energy installation. The choice of the material is critical for design considerations and for optimal performance. Usually we want to maximize the heat storage capacity (HSC) and minimize the liquidus temperature. The HSC is defined as the ability of the system to store energy per unit volume. In practice, the HSC is defined by the ratio

$$\text{HSC} = \frac{C_{m,P}}{V_m}$$

where $C_{m,P} = \frac{\partial H}{\partial T}$ is the molar heat capacity at constant pressure describing the change in the energy at atmospheric pressure, H , with temperature, and V_m is the molar volume. HSC is in general a smooth function of the composition, but it may exhibit abrupt changes in the vicinity of a phase transition.

The liquidus temperature T_{liq} is the temperature above which a chemical system is completely in the liquid state. Below T_{liq} , one or more solid phases (stoichiometric or nonstoichiometric or solutions) are in thermodynamic equilibrium with the liquid. Above T_{liq} , the system is a homogeneous liquid solution.

From the optimization point of view, the determination of the composition of the minimum liquidus temperature is a good example for testing the capability of a blackbox optimization algorithm for which the blackbox is **FactSage**. Indeed, the liquidus temperature is a complex function of the global composition, especially when a large number of solid phases are involved in the system. From a mathematical point of view, T_{liq} is a continuous nonsmooth function of the composition. In addition, T_{liq} may have many local extrema and saddle points. It is usually almost impossible to give a clear graphical representation of the topology of T_{liq} for a system with more than three constituents. T_{liq} is also a typical blackbox function because it results from the Gibbs energy minimization of the system, which is a search for the temperatures at which the liquid phase is in equilibrium with the solid phases. For further information on these calculations see [32].

In the current example, we consider the six-component system of chlorides: LiCl – NaCl – KCl – MgCl₂ – CaCl₂ – MnCl₂. Note that the main **FactSage** limitation is actually a database limitation, and extrapolation methods are used for the thermodynamic description of the systems for which no data are available. These methods are described in [25, 28].

The optimization problem is to simultaneously minimize the liquidus temperature and maximize the HSC ($f^{(1)} = T_{liq}$ and $f^{(2)} = -\text{HSC}$). The $n = 5$ optimization variables are the weight percentages of the

composition, denoted X_e with $e \in \{\text{LiCl}, \text{NaCl}, \text{KCl}, \text{MgCl}_2, \text{CaCl}_2\}$ and bounds $[0, 100]$. The weight percentage of MnCl_2 is implicitly determined via $100 - \sum_{i=1}^5 X_i$; it is not controlled by BiMADS. Two linear constraints $0 \leq 100 - \sum_{i=1}^5 X_i \leq 100$ ensure that the quantity is feasible. We have compared the results obtained by BiMADS and the popular NSGA-II genetic algorithm [16] with a budget of 3,000 blackbox evaluations. The two approximated Pareto fronts are plotted in Figure 3, and the compositions minimizing the liquidus temperature are listed in Table 1. The table also gives the improved composition (in terms of T_{liq}) obtained after 50,000 LHS evaluations.

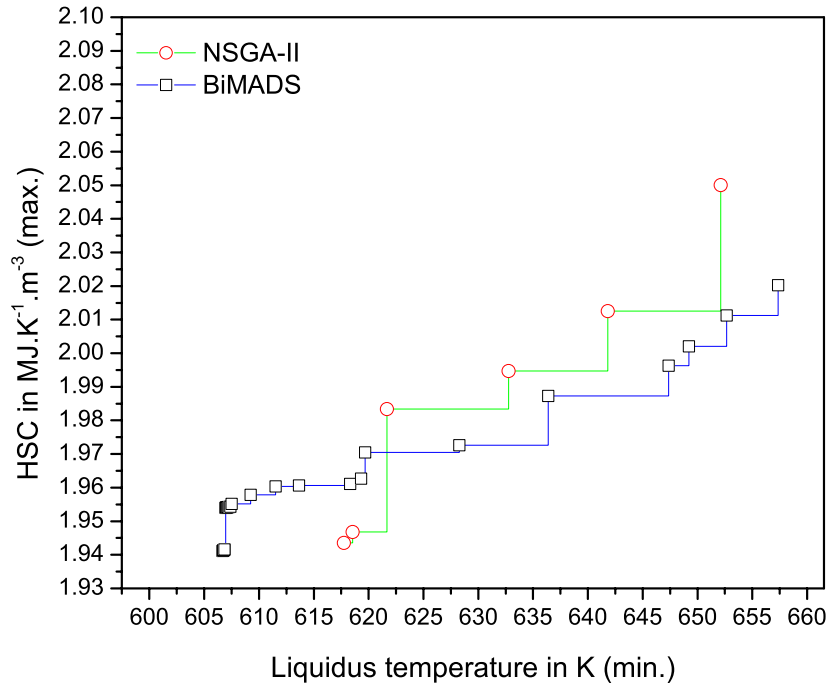


Figure 3: Approximated Pareto fronts of alloy compositions, obtained by the BiMADS and the NSGA-II methods, simultaneously minimizing the liquidus temperature ($T_{liq} = f^{(1)}$) and maximizing the heat storage capacity ($\text{HSC} = -f^{(2)}$).

Table 1: Compositions minimizing the liquidus temperature obtained along the approximated Pareto front of Figure 3, along with the two objective functions and the number of blackbox evaluations, for the $\text{LiCl} - \text{NaCl} - \text{KCl} - \text{MgCl}_2 - \text{CaCl}_2 - \text{MnCl}_2$ system.

Algo.	Values	X_{LiCl}	X_{NaCl}	X_{KCl}	X_{MgCl_2}	X_{CaCl_2}	MnCl_2	$T_{liq} (f^{(1)})$	$\text{HSC} (-f^{(2)})$	Blackbox evaluations
	(wt.%)	(wt.%)	(wt.%)	(wt.%)	(wt.%)	(wt.%)	(K)	($\text{MJ.K}^{-1}.\text{m}^{-3}$)		
BiMADS		5.938	18.067	14.719	14.235	15.300	31.740	606.7	1.941	3,000
NSGA-II		5.747	20.457	13.467	14.464	16.729	29.135	617.7	1.943	3,000
LHS		24.000	9.000	41.000	11.000	10.000	5.000	653.0	1.905	50,000

From Figure 3, BiMADS generated more nondominated points for smaller values of T_{liq} , providing a richer approximation to the Pareto front than NSGA-II achieved. NSGA-II could however generate a few nondominated solutions with better values for HSC. However, from an industrial point of view, these solutions do not improve on other solutions found by BiMADS with better T_{liq} values: to increase the HSC by 1% (from 1.96 to 2.00) we must increase the liquidus temperature by 20 K.

We now consider the solution quality. There is no physical criterion for the existence of an extremum for HSC. However, it is particularly significant that the best solution found by BiMADS, for the first objective, is a local minimum of the liquidus temperature in the thermodynamic sense. Such a minimal value of T_{liq} is called the *eutectic temperature*, denoted T_E .

The proof is as follows: According to classical thermodynamic rules, for a given real $\varepsilon > 0$, at $T_E - \varepsilon$, only solid phases can be present, while at $T_E + \varepsilon$, the system must be a homogeneous liquid phase. A heat release must also be observed at this minimum, i.e., $\Delta H(T_{liq} + \varepsilon) - \Delta H(T_{liq} - \varepsilon)$ must be a relatively large value of several kJ.kg^{-1} . At the composition found by BiMADS, for $\varepsilon = 0.66 \text{ K}$, we found that 1 kg of liquid gives 6 solids in equilibrium with a corresponding heat release of 256 kJ.kg^{-1} , which proves the phase transition from a single liquid phase to solids, and thus that BiMADS has provided a eutectic temperature. The solutions found by LHS and NSGA-II that minimize the liquidus temperature are not local minima because below the obtained minimum temperature, solids are found to be in equilibrium with the liquid.

4 Production of aluminum in Hall–Héroult cells

Aluminum is produced by the electro-reduction of alumina (Al_2O_3) in Hall–Héroult cells. The alumina fed to the electrolysis cell dissolves in a bath consisting mainly of molten cryolite (Na_3AlF_6) at an operating temperature of about 960°C . Upon electrolysis, Al^{3+} ions are reduced to liquid Al at the cathode, and O^{2-} ions through oxidation and reaction with the carbon of the consumable anodes form $\text{CO}_2(\text{gas})$ at the anode. A Hall–Héroult electrolysis cell is shown schematically in Figure 4. The global reaction of the electrolysis is:

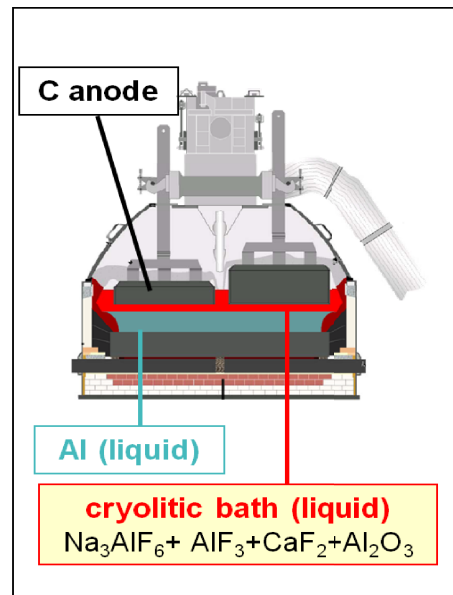
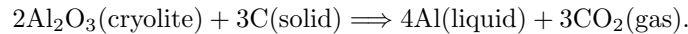


Figure 4: Simplified representation of the Hall–Héroult electrolysis cells and the chemical composition of the cryolitic bath.

4.1 Problem description

The base electrolyte is $\text{Na}_3\text{AlF}_6 - \text{AlF}_3 - \text{CaF}_2 - \text{Al}_2\text{O}_3$ (i.e., $\text{NaF} - \text{AlF}_3 - \text{CaF}_2 - \text{Al}_2\text{O}_3$ system). Additions of AlF_3 and CaF_2 decrease the liquidus temperature of the electrolyte [24], thus lowering the operating temperature. According to Chrenkova *et al.* [11], a typical electrolyte consists of Na_3AlF_6 with additions of (6–13) weight percentage (wt.%) AlF_3 , (3–8) wt.% CaF_2 , and (2–5) wt.% Al_2O_3 , with an operating temperature lying between 945°C and 970°C . The bath ratio (BR), defined as the NaF/AlF_3 mass ratio, usually lies in the range 0.9–1.3. Consider a “typical” base electrolyte with $\text{BR}=1.1$, 5 wt.% CaF_2 , and 2.5 wt.% Al_2O_3 at 960°C . Its calculated density is about 2.08 g.cm^{-3} [29] whereas the density of pure liquid aluminum is about 2.30 g.cm^{-3} [24] at the same temperature. As emphasized by Haupin [24], the difference in density between the electrolyte and liquid aluminum is small, and therefore small disturbances can cause considerable movement of the aluminum-electrolyte interface. Increasing the density difference by

reducing the electrolyte density will ensure a good aluminum/electrolyte separation. Moreover, an increase in the electrical (ionic) conductivity of the electrolyte will improve the energy efficiency of the electrolytic process. Therefore, it is highly desirable to simultaneously minimize the density and maximize the electrical conductivity of the electrolyte.

We define an optimization model in which the variables correspond to the weight percentages of the components of the system NaF, AlF₃, CaF₂, and Al₂O₃, giving $n = 3$ variables denoted X_e with $e \in \{\text{NaF}, \text{AlF}_3, \text{CaF}_2\}$. The remaining element (Al₂O₃) is determined implicitly since the sum of the weight percentages must equal 100.

A thermodynamic model for the NaF – AlF₃ – CaF₂ – Al₂O₃ base system was developed in [10]. The modified quasichemical model (MQM) in the quadruplet approximation [27], which evaluates the coupled first-nearest-neighbor and second-nearest-neighbor short-range order, was used for the molten salt phase. The model parameters were obtained mainly by the critical evaluation and optimization of available thermodynamic and phase-equilibrium data for the binary and ternary subsystems [10]. The model was then used to estimate the thermodynamic properties of the multicomponent system from these assessed binary and ternary parameters using interpolation methods. In particular, the liquidus temperature, Al₂O₃ solubility, and vapor pressure were calculated. More recently, theoretical models based on the MQM have been developed for the density [29–31] and electrical conductivity (unpublished results) of multicomponent inorganic liquids. These have been successfully applied to the NaF – AlF₃ – CaF₂ – Al₂O₃ electrolyte [29]. Given the developed thermodynamic and physical-property databases, the liquidus temperature, density, and electrical conductivity of the electrolyte can be calculated. This is done by the FactSage software (and its databases), which is seen as a blackbox.

We used the BiMADS algorithm and NOMAD to simultaneously minimize the density and maximize the electrical conductivity, while respecting the following constraints on the operating temperature and on the global composition of the electrolyte:

$$\begin{cases} \text{Operating temperature } (T) = \text{liquidus temperature} + 5^\circ\text{C} \leq 970^\circ\text{C}. \\ 0.6 \leq \text{BR} = X_{\text{NaF}}/X_{\text{AlF}_3} \leq 1.3. \\ \text{Bounds on the quantity of Al}_2\text{O}_3: 2 \leq 100 - X_{\text{NaF}} - X_{\text{AlF}_3} - X_{\text{CaF}_2} \leq 5. \end{cases}$$

The two variables X_e with $e \in \{\text{NaF}, \text{AlF}_3\}$ are taken in $[0, 100]$ and X_{CaF_2} must be in $[3, 10]$.

4.2 Numerical results

In this example, we used the VNS and LHS searches with a budget of 500 evaluations. Of the 500 calculations, 100 were performed in an initial LHS search. The approximated Pareto front, maximum ionic conductivity versus minimum density, is shown in Figure 5. The composition (and thus the liquidus temperature) of the electrolyte changes along this front. The calculated composition (expressed as a weight percentage) along the front as a function of the calculated optimal density and ionic conductivity is shown in Figures 6 and 7. Finally, the calculated compositions and operating temperatures of the characteristic points A, B, C, and D defined in Figure 5 are given in Table 2.

Table 2: Calculated compositions and operating temperatures of the characteristic points of the approximated Pareto front in Figure 5.

Quantity	A	B	C	D	“typical” electrolyte
BR	0.62	0.88	1.09	1.30	1.10
X_{CaF_2} (wt.%)	3.5	3.0	3.0	10.0	5.0
Al ₂ O ₃ (wt.%)	5.0	3.7	2.0	2.0	2.5
T (°C)	944	890	970	969	964

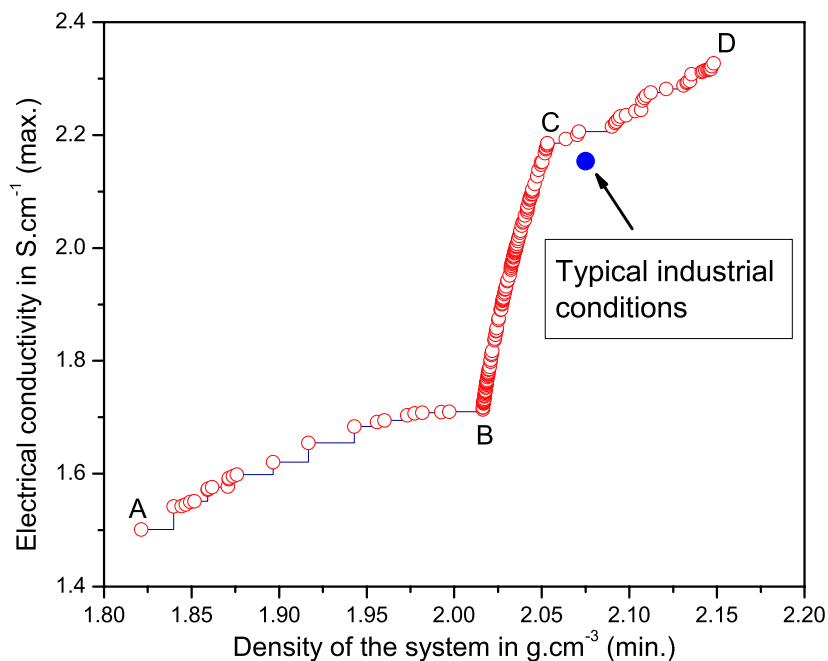


Figure 5: Approximated Pareto front representing the optimal composition that minimizes the density ($f^{(1)}$) and maximizes the ionic conductivity ($-f^{(2)}$) of the NaF – AlF₃ – CaF₂ – Al₂O₃ electrolyte.

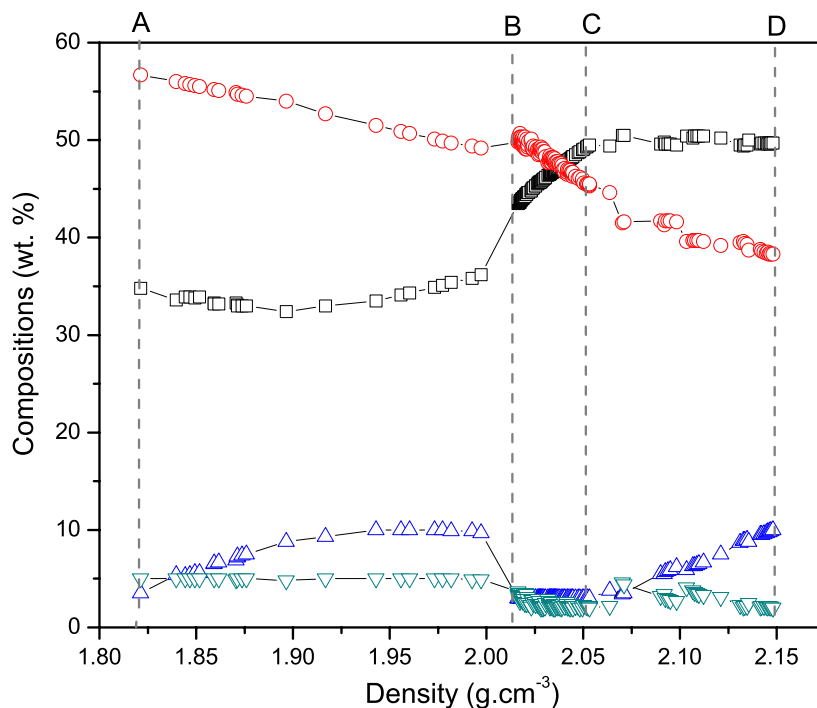


Figure 6: Calculated compositions of the NaF – AlF₃ – CaF₂ – Al₂O₃ electrolyte along the approximated Pareto front shown in Figure 5 as a function of density. Black squares correspond to NaF, red circles to AlF₃, blue triangles to CaF₂, and inverted triangles to Al₂O₃.

The dramatic increase in ionic conductivity observed between points B and C in the Pareto front is due to the following combined effects: (1) increase in BR (i.e., increase in the basicity of the electrolyte), (2) decrease in the Al₂O₃ content, and (3) increase in the operating temperature.

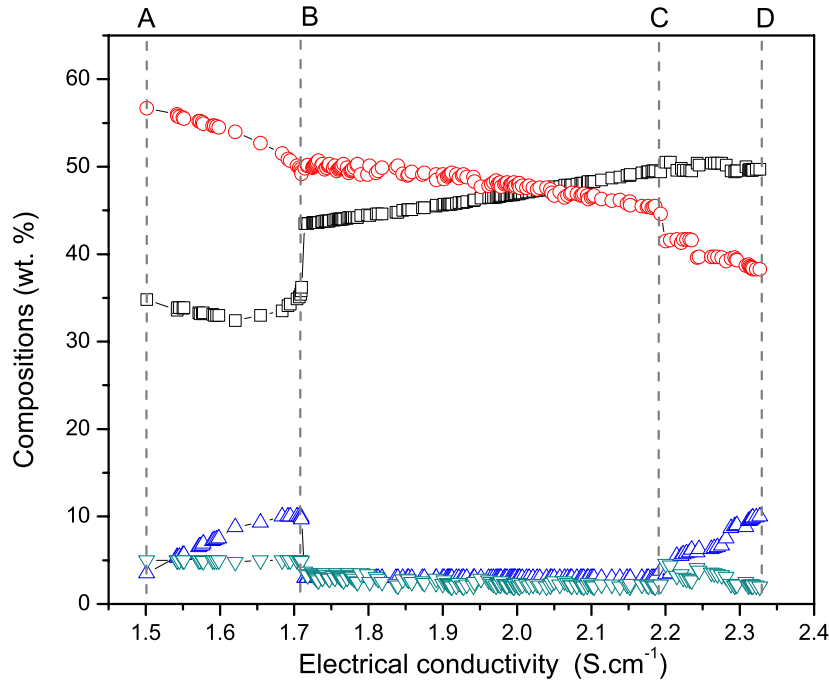


Figure 7: Calculated compositions of the NaF – AlF₃ – CaF₂ – Al₂O₃ electrolyte along the approximated Pareto front shown in Figure 5 as a function of ionic conductivity. Black squares correspond to NaF, red circles to AlF₃, blue triangles to CaF₂, and inverted triangles to Al₂O₃.

On the one hand, these three effects are cumulative for the ionic conductivity (they all increase it), which explains the important ionic conductivity change (about 0.47 S.cm^{-1}) observed between points B and C. On the other hand, the three effects partly cancel each other for the density: effects (1) and (2) both increase the density while effect (3) decreases it. Hence, the density change observed between points B and C is moderate (only about 0.04 g.cm^{-3}). Also, the range of density values accessible to the electrolyte is much more limited than the range of ionic conductivity values. As shown in Figure 5, we were able to obtain alternative operating conditions. In particular, the electrolyte at point C seems promising compared to the “typical” electrolyte. Although it is slightly poorer in Al₂O₃ (2.0 instead of 2.5 wt.%), it contains less CaF₂ (3.0 instead of 5.0 wt.%) and has virtually the same BR value (1.09 instead of 1.10). It has a liquidus temperature only about 6°C higher, along with a lower density (by about 0.02 g.cm^{-3}) and a higher electrical conductivity (by about 0.03 S.cm^{-1}).

5 Design of new steel

In recent years, as the price of fossil-fuel energy has increased, and because of environmental concerns, the automotive industry has shown more and more interest in designing lighter engines and body parts. Accordingly, an important research area is the manufacture of ultra-high-strength steels for automotive panel applications using precipitation hardening. Significant precipitation hardening can be achieved in a martensite matrix [17]. Martensite is a form of steel crystalline structure that crystallizes in a body-centered tetragonal structure. It results from the distortion of the face-centered cubic lattice of austenite during the quenching. Maraging steel [18, 33] is such a potential new steel; however, it requires large quantities of expensive additives such as Co and Ni, which is not viable for the automotive industry. Can we make a low-cost precipitation-hardenable alloy starting from a martensite matrix?

5.1 Problem description

The optimization formulation is based on an approach communicated to us by two metallurgical experts, Christopher Hutchinson (christopher.hutchinson@monash.edu) and Chad Sinclair (chad.sinclair@ubc.ca). This approach is based on the development of a two-phase mixture that is inherently resistant to coarsening. The minor phase (austenite) was found to coarsen at a very slow rate that is controlled by the bulk diffusion of substitutional elements in the parent phase. Grain growth within the predominant phase (ferrite) was fixed by the minor phase. To take advantage of the two-phase mixture, it is necessary to develop a chemistry for which the austenite and ferrite phases co-exist over a wide range of temperatures.

The simulation tool used for this application is organized around two blackboxes corresponding to two independent software packages running in parallel and wrapped into a single blackbox interfaced with NOMAD. The first component is the FactSage software and its databases, and the second is the *Sourmail neural network blackbox* for the estimation of T_s , the martensite start temperature in °C [34]. The overall optimization scheme is presented in Figure 8.

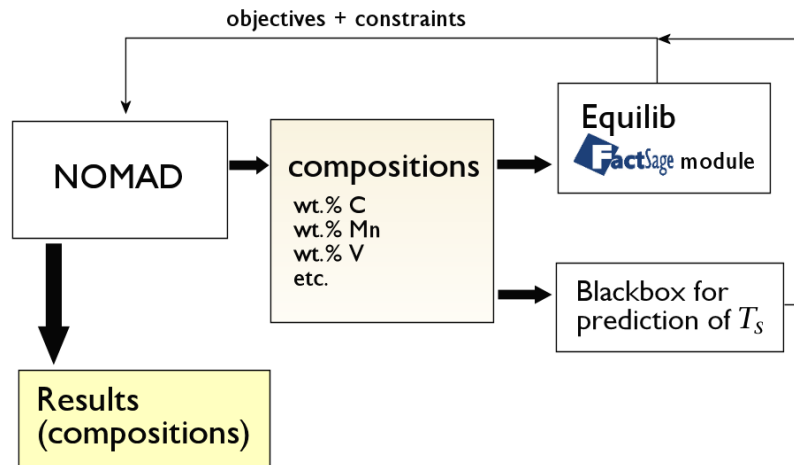


Figure 8: Optimization scheme using two blackboxes.

The associated optimization problem maximizes the following two objectives:

$$\begin{cases} f^{(1)} = -M_{\text{Fe}} \\ f^{(2)} = -M_{P_{\text{mart}}} \end{cases}$$

where M_{Fe} is the mass of iron for 100 g of alloy, in g, and $M_{P_{\text{mart}}}$ is the mass of precipitate in martensite per 100 g of alloy at 25°C, in g. The first objective is a linear function of the compositions; maximizing the amount of Fe decreases the cost of the alloy. The second objective is obtained by the blackbox.

There are $n = 12$ optimization variables corresponding to the weight percentage (wt.%) of the possible alloy elements. They are expressed as X_e for element e , and they are listed in Table 3, along with their bounds (the composition ranges).

Since we want to keep the carbon content low to avoid problems with welding, the upper bound of X_{C} is set to 0.03. Note also that elemental iron, which is associated with the first objective, does not appear as a variable. As in the first two examples, since the compositions must sum to 100%, it is implicitly expressed in the interface of the blackbox as $100 - \sum_{i=1}^{12} X_i$. Its range is expressed not as a bound but as two linear constraints.

Other constraints are given by the blackbox. First, we must be able to get 100% austenite at temperatures somewhere in the range 800–1200°C, so that when we quench we get a martensite matrix to start with. We model this constraint by $M_{\text{aust}} \geq 99.99\%$ where M_{aust} is the mass of austenite per 100 g of alloy, in g. Second,

Table 3: Optimization variables: Possible alloy elements and their composition ranges.

Element (wt.%)	Lower bound	Upper bound
X_C	0	0.03
X_{Mn}	0	4
X_V	0	2
X_{Ni}	0	10
X_{Ti}	0	2
X_{Mo}	0	6
X_{Cu}	0	3
X_{Co}	0	10
X_{Al}	0	3
X_{Si}	0	2
X_{Nb}	0	0.5
X_{Cr}	0	10

we need to form a significant amount of precipitate (at least 3–5%) in an intermetallic second phase in the martensite matrix, so we have the potential for precipitate hardening, in the temperature range 400–600°C. This is modeled by $M_{mart} + M_{P_{mart}} \geq 99.99\%$ where M_{mart} is the mass of martensite for 100 g of alloy, in g. Finally, for kinetic reasons the martensite start temperature has to be above 400°C: $T_s \geq 400$.

5.2 Numerical results

The optimization is quite tedious, because 12 variables are involved and each calculation with FactSage can take several minutes because of the many phases involved. A brute-force method, i.e., an explicit enumeration with an accuracy of 0.5 wt.% (lower than the maximum limit of C and the quantity of N), would require about 6 million FactSage calculations. This is not possible in a reasonable time.

In NOMAD, we set the maximum number of blackbox calculations to 20,000. Of these, 5,000 were performed in an initial LHS search. This represents roughly one week of calculations on a standard desktop computer. The approximation of the Pareto front provided by NOMAD is shown in Figure 9.

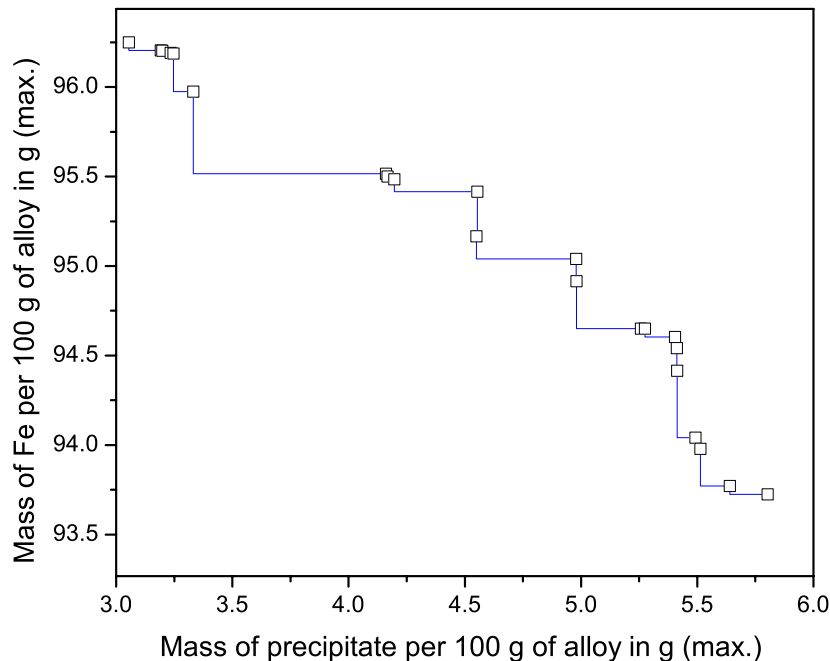


Figure 9: Approximated Pareto front of alloy compositions, simultaneously maximizing the wt.% of Fe and the mass of precipitate in the ferrite matrix at room temperature.

NOMAD generated 23 nondominated compositions. This number may appear low given that the Pareto front is not densely populated. This can be explained by the fact that “only” 20,000 calculations were performed. NOMAD was able to identify the regions where the constraints are satisfied and to generate nondominated compositions within these regions. In this example, the most important task was to identify the narrow composition region where the constraints are satisfied. In this sense, the result of this optimization is remarkable. Future work could improve the optimization by replacing the initial LHS search with starting points that belong to the previous approximation of the Pareto front, thus obtaining even more compositions in the targeted regions.

6 Discussion

We have described complex industrial applications involving new alloys and process design. Each uses a blackbox based on the FactSage software; no derivative information is available for the optimization. The other characteristics include two objectives and nonlinear blackbox constraints. We applied the BiMADS algorithm to these examples using the NOMAD software. In the first example (Section 3), it cannot be rigorously proved that a global minimum in terms of liquidus temperature was achieved, but thermodynamics arguments provided some information. In the second example (Section 4), we found a new composition for the cryolitic bath that can potentially improve the efficiency of Hall–Héroult cells. The third example (Section 5) is very difficult because of the large number of potential alloy elements and the very narrow single-phase region constraint. The fact that BiMADS could find feasible compositions is useful information. Overall, the BiMADS algorithm was found to be efficient and robust for these real applications, in the presence of functions with a complex structure, several local minima, singularities, and rapid variation over a narrow range of compositions. The first example also justified our choice of BiMADS over the popular genetic algorithm NSGA-II.

References

- [1] M.A. Abramson, C. Audet, G. Couture, J.E. Dennis, Jr., S. Le Digabel, and C. Tribes. The NOMAD project. Software available at <https://www.gerad.ca/nomad>.
- [2] M.A. Abramson, C. Audet, J.E. Dennis, Jr., and S. Le Digabel. OrthoMADS: A deterministic MADS instance with orthogonal directions. *SIAM Journal on Optimization*, 20(2):948–966, 2009.
- [3] C. Audet, V. Béchar, and S. Le Digabel. Nonsmooth optimization through mesh adaptive direct search and variable neighborhood search. *Journal of Global Optimization*, 41(2):299–318, 2008.
- [4] C. Audet and J.E. Dennis, Jr. Mesh adaptive direct search algorithms for constrained optimization. *SIAM Journal on Optimization*, 17(1):188–217, 2006.
- [5] C. Audet and J.E. Dennis, Jr. A progressive barrier for derivative-free nonlinear programming. *SIAM Journal on Optimization*, 20(1):445–472, 2009.
- [6] C. Audet, J.E. Dennis, Jr., and S. Le Digabel. Globalization strategies for mesh adaptive direct search. *Computational Optimization and Applications*, 46(2):193–215, 2010.
- [7] C. Audet, G. Savard, and W. Zghal. Multiobjective optimization through a series of single-objective formulations. *SIAM Journal on Optimization*, 19(1):188–210, 2008.
- [8] C. Audet, G. Savard, and W. Zghal. A mesh adaptive direct search algorithm for multiobjective optimization. *European Journal of Operational Research*, 204(3):545–556, 2010.
- [9] C.W. Bale, E. Bélisle, P. Chartrand, S.A. Decterov, G. Eriksson, K. Hack, I.-H. Jung, Y.-B. Kang, J. Melançon, A.D. Pelton, C. Robelin, and S. Petersen. FactSage thermochemical software and databases – recent developments. *CALPHAD: Computer Coupling of Phase Diagrams and Thermochemistry*, 33(2):295–311, 2009.
- [10] P. Chartrand and A.D. Pelton. A predictive thermodynamic model for the Al-NaF-AlF₃-CaF₂-Al₂O₃ system. In W.A. Schneider, editor, *Light Metals 2002*, pages 245–252. Minerals, Met. & Mat. Soc., 2002.
- [11] M. Chrenkova, V. Danek, A. Silny, and T.A. Utigard. Density, electrical conductivity and viscosity of low melting baths for aluminium electrolysis. In W. Hale, editor, *Light Metals 1996*, pages 227–232. Minerals, Met. & Mat. Soc., 1996.
- [12] F.H. Clarke. *Optimization and Nonsmooth Analysis*. John Wiley & Sons, New York, 1983. Reissued in 1990 by SIAM Publications, Philadelphia, as Vol. 5 in the series *Classics in Applied Mathematics*.

- [13] A.R. Conn and S. Le Digabel. Use of quadratic models with mesh-adaptive direct search for constrained black box optimization. *Optimization Methods and Software*, 28(1):139–158, 2013.
- [14] A.R. Conn, K. Scheinberg, and L.N. Vicente. *Introduction to Derivative-Free Optimization*. MOS-SIAM Series on Optimization. SIAM, Philadelphia, 2009.
- [15] A.L. Custódio, J.F.A. Madeira, A.I.F. Vaz, and L.N. Vicente. Direct multisearch for multiobjective optimization. *SIAM Journal on Optimization*, 21(3):1109–1140, 2011.
- [16] K. Deb, A. Pratap, S. Agarwal, and T. Meyarivan. A fast and elitist multiobjective genetic algorithm: NSGA-II. *IEEE Transactions on Evolutionary Computation*, 6(2):182–197, 2002.
- [17] E.P. Degarmo, J.T. Black, and R.A. Kohser. *Materials and Processes in Manufacturing*. John Wiley & Sons, 9th edition, 2003.
- [18] O. Dmitrieva, D. Ponge, G. Inden, J. Millán, P. Choi, J. Sietsma, and D. Raabe. Chemical gradients across phase boundaries between martensite and austenite in steel studied by atom probe tomography and simulation. *Acta Materialia*, 59(1):364–374, 2011.
- [19] E. Fermi and N. Metropolis. Numerical solution of a minimum problem. Los Alamos Unclassified Report LA-1492, Los Alamos National Laboratory, Los Alamos, USA, 1952.
- [20] R. Fletcher and S. Leyffer. Nonlinear programming without a penalty function. *Mathematical Programming, Series A*, 91:239–269, 2002.
- [21] A.E. Gheribi, C. Audet, S. Le Digabel, E. Bélisle, C.W. Bale, and A.D. Pelton. Calculating optimal conditions for alloy and process design using thermodynamic and properties databases, the FactSage software and the mesh adaptive direct search algorithm. *CALPHAD: Computer Coupling of Phase Diagrams and Thermochemistry*, 36:135–143, 2012.
- [22] A.E. Gheribi, S. Le Digabel, C. Audet, and P. Chartrand. Identifying optimal conditions for magnesium based alloy design using the mesh adaptive direct search algorithm. *Thermochimica Acta*, 559:107–110, 2013.
- [23] A.E. Gheribi, C. Robelin, S. Le Digabel, C. Audet, and A.D. Pelton. Calculating all local minima on liquidus surfaces using the FactSage software and databases and the mesh adaptive direct search algorithm. *The Journal of Chemical Thermodynamics*, 43(9):1323–1330, 2011.
- [24] W. Haupin. The influence of additives on Hall-Héroult bath properties. *JOM*, 43(11):28–34, 1991.
- [25] L. Kaufman and H. Bernstein. *Computer Calculation of Phase Diagrams*. Academic Press, New York, 1970.
- [26] S. Le Digabel. Algorithm 909: NOMAD: Nonlinear optimization with the MADS algorithm. *ACM Transactions on Mathematical Software*, 37(4):44:1–44:15, 2011.
- [27] A.D. Pelton, P. Chartrand, and G. Eriksson. The modified quasi-chemical model: Part IV. Two-sublattice quadruplet approximation. *Metallurgical and Materials Transactions A*, 32(6):1409–1416, 2001.
- [28] E. Renaud, C. Robelin, A.E. Gheribi, and P. Chartrand. Thermodynamic evaluation and optimization of the Li, Na, K, Mg, Ca, Sr, F, Cl reciprocal system. *Journal of Chemical Thermodynamics*, 43(8):1286–1298, 2011.
- [29] C. Robelin and P. Chartrand. A density model based on the modified quasichemical model and applied to the NaF-AlF₃-CaF₂-Al₂O₃ electrolyte. *Metallurgical and Materials Transactions B*, 38(6):881–892, 2007.
- [30] C. Robelin and P. Chartrand. Predictive models for the density and viscosity of the NaF-AlF₃-CaF₂-Al₂O₃ electrolyte. In M. Sorlie, editor, *Light Metals 2007*, pages 565–570. Minerals, Met. & Mat. Soc., 2007.
- [31] C. Robelin, P. Chartrand, and G. Eriksson. A density model for multicomponent liquids based on the modified quasichemical model: Application to the NaCl-KCl-MgCl₂-CaCl₂ system. *Metallurgical and Materials Transactions B*, 38(6):869–879, 2007.
- [32] N. Saunders and A.P. Miodownik, editors. Chapter 6: Phase Stabilities, volume 1 of *Pergamon Materials Series*. Pergamon, 1998.
- [33] W. Sha. Ultra high-strength maraging steel. In *Steels*, pages 141–161. Springer, 2013.
- [34] T. Sourmail. Predicting the martensite start temperature (Ms) of steels. <http://www.thomas-sourmail.net/martensite.html>, 2014.
- [35] S. Tiwaria, G. Fadelb, and K. Deb. AMGA2: Improving the performance of the archive-based micro-genetic algorithm for multi-objective optimization. *Engineering Optimization*, 43(4):377–401, 2011.
- [36] V. Torczon. On the convergence of pattern search algorithms. *SIAM Journal on Optimization*, 7(1):1–25, 1997.